

DEBOSH: Deep Bayesian Shape Optimization

Nikita Durasov,¹ Artem Lukoyanov,² Jonathan Donier,² Pascal Fua¹

¹Computer Vision Laboratory, EPFL, {name.surname}@epfl.ch

²Neural Concept SA, {name.surname}@neuralconcept.com

<https://nikitadurasov.github.io/projects/debosh/>

Abstract

Shape optimization is at the heart of many industrial applications, such as aerodynamics, heat transfer, and structural analysis. It has recently been shown that Graph Neural Networks (GNNs) can predict the performance of a shape quickly and accurately and be used to optimize more effectively than traditional techniques that rely on response-surfaces obtained by Kriging. However, GNNs suffer from the fact that they do not evaluate their own accuracy, which is something Bayesian Optimization methods require. Therefore, estimating confidence in generated predictions is necessary to go beyond straight deterministic optimization, which is less effective.

In this paper, we demonstrate that we can use Ensembles-based technique to overcome this limitation and outperform the state-of-the-art. Our experiments on diverse aerodynamics and structural analysis tasks prove that adding uncertainty to shape optimization significantly improves the quality of resulting shapes and reduces the time required for the optimization.

1 Introduction

Simulation is a powerful tool to refine the 3D shape of a design. For example, Computational Fluid Dynamics (CFD) is central to maximizing the performance of aircraft wings, windmill blades, hydrofoils, car bodies, ship hulls, and propellers, while Structural Analysis is key to designing structures that are both light and strong. In both cases, because the simulation must be re-run each time the design is changed, a widespread engineering practice is to test only a few designs, without searching the design space. The same can be said in many other fields, such as heat transfer management or electronic component design, that involve complicated simulations to optimize shapes.

One way to explore the shape space more thoroughly is to use genetic algorithms (Gosselin, Tye-Gingras, and Mathieu-Potvin 2009). However, in their simplest form, they require many evaluations of a fitness function and therefore many expensive simulations, which makes them inefficient. Relying on *Kriging*, also known as Gaussian-process (GP) regression (Rasmussen and Williams 2006), is one of the most popular ways to reduce the required number of evaluations (Jeong, Murayama, and Yamamoto 2005; Laurenceau

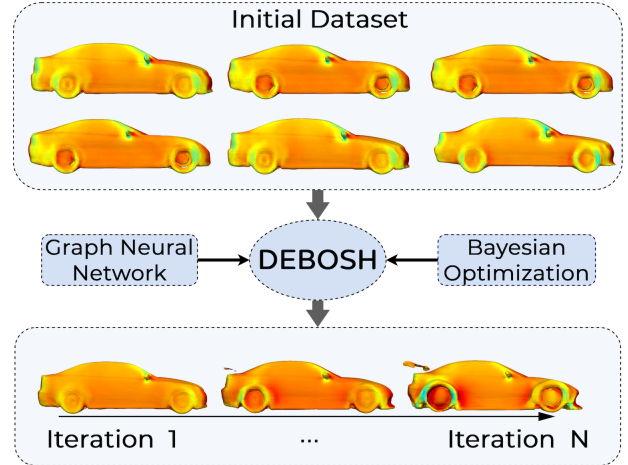


Figure 1: **Shape Optimization.** Starting from 3D shapes in initial training dataset, *DEBOSH* uses a GCNN to compute a response surface and Bayesian Optimization to efficiently produce an optimized shape that it has never seen before.

et al. 2010; Toal and Keane 2011; Xu et al. 2017). Unfortunately, Kriging works best for models that can be parameterized using relatively few parameters, which limits its applicability.

Other methods rely on topology optimization (Saviers, Ranjan, and Mahmoudi 2019) or adjoint differentiation (Allaire 2015; Gao, Wu, and Xia 2017; Behrou, Ranjan, and Guest 2019). The first is highly effective but only applicable in very specific cases, while the second approximates the solution of a so-called *adjoint* form of the partial differential equations to compute the gradients of the fitness function with respect to the 3D simulation mesh. However, this only applies to relatively small deformations with respect to an original shape and requires careful re-meshing of the shape and re-running the simulation once the changes exceed a threshold. Furthermore, this method is even more computationally expensive than those discussed above (Alexandersen, Sigmund, and Aage 2016).

A radically different approach was proposed in (Baqué et al. 2018): Given a collection of 3D surface meshes and corresponding results of simulations, it is possible to train a Geodesic Convolutional Neural Networks (GC-

NNs) (Boscaini et al. 2016; Monti et al. 2017) to emulate a complex fluid-dynamics simulator. This makes it possible to write a differentiable objective function that returns aerodynamic and hydrodynamic properties—drag, lift, stability—very fast and therefore to maximize performance with respect to the 3D shape of the target objects, no matter how many parameters are required to define its shape. That gives it an edge over Kriging that can only deal with relatively fewer parameters. However, unlike Kriging, it suffers from the fact that it does not account for the potential imprecision of its prediction.

To remedy this, we introduce a new Bayesian shape optimization algorithm, which we dub *DEBOSH*. We start with the GCNN of (Baq   et al. 2018) and give it the ability to estimate its own uncertainty using an ensemble-based approach similar to (Lakshminarayanan, Pritzel, and Blundell 2017; Gal and Ghahramani 2016a; Durasov et al. 2021; Wen, Tran, and Ba 2020). This enables us to rely on Bayesian Optimization (BO) to explore the shape space and re-train the network when necessary to produce shapes such as the one depicted by Fig. 1. As a result *DEBOSH* outperforms both earlier deep learning and classical approaches in terms of quality of the optimized shapes and required time to obtain them, which we demonstrate on several benchmarks.

2 Related Work

In all engineering fields that rely on running computationally demanding simulations on 3D shapes to estimate their performance, optimizing these shapes to maximize this performance is a difficult problem because, in practice, the simulator can only be run so many times. In this section, we briefly review some of the dominant approaches to addressing this problem. We also introduce standard Bayesian Optimization, which we will rely on in the method section.

2.1 Shape Optimization

A popular way to automate the shape optimization processes is to use genetic algorithms (Gosselin, Tye-Gingras, and Mathieu-Potvin 2009) to explore the shape space. However, as genetic algorithms require many evaluations of the fitness function, which involves running an expensive physical simulation, a naive implementation would be inefficient. *Kriging*, or Gaussian-process (GP) regression (Rasmussen and Williams 2006), is one of the most popular ways to reduce the required number of evaluations (Jeong, Murayama, and Yamamoto 2005; Laurenceau et al. 2010; Toal and Keane 2011; Xu et al. 2017; Umetani and Bickel 2018). It estimates a response surface that is used to accelerate the exploration of the shape space. Although effective when dealing with models controlled by relatively few design parameters, it does not scale well to high-dimensional inputs or to sparse GPs (Herbrich, Lawrence, and Seeger 2003), due to the *curse of dimensionality* (Bellman 1961). As a result, these methods often depend on handcrafted low-dimensional shape parameterizations that can be difficult to design and severely restrict how much of the shape space can be explored.

To alleviate this problem, it has been proposed to apply deep learning methods (Vaswani et al. 2017; Chen et al.

2017; Redmon et al. 2016; Durasov et al. 2019) and Convolutional Neural Networks (CNNs) in 3D voxelized grids. This has been used to accelerate the search for solutions of the discrete Poisson equation (Tompson et al. 2017), to directly regress the fluid velocity fields given an implicit surface description (Guo, Li, and Iorio 2016), or to compute fluid simulations velocities from a set of reduced parameters (Kim et al. 2019). However, the underlying 3D CNN architectures working with spatial voxels tend to feature large memory footprints and computationally demanding inference. To work around this problem, it has been proposed to replace the GPs with Geodesic Convolutional Neural Networks (GCNNs) (Boscaini et al. 2016; Monti et al. 2017) to emulate a simulator (Baq   et al. 2018; Remelli et al. 2020). Given a set of generic surfaces parametrized as meshes, a GCNN is trained to predict their aerodynamic characteristics, as computed by standard CFD packages (Drela 1989; Weller et al. 1998; Mountrakis et al. 2015). These characteristics are then used to write an objective function that is differentiable with respect to the shape parameters. To maximize performance, the objective function is minimized with respect to these parameters. This makes it possible to deal with more complex parameterization but fails to estimate uncertainties, which hampers the use of so-called exploration-and-exploitation algorithms such as those discussed below, which are very powerful for these kinds of applications (Laurenceau et al. 2010).

2.2 Bayesian Optimization

Bayesian Optimization (BO) (Mockus 2012) is an exploration-and-exploitation approach to finding global minima of a multivariate function $g : \mathbf{A} \rightarrow \mathbb{R}$ that does not assume any specific functional form for g and is usually used for functions that are expensive to evaluate. In our application g is implemented by a physics-based simulator.

BO typically starts with a surrogate model $\tilde{g}_\Theta : \mathbf{A} \rightarrow \mathbb{R}$ whose output depends on a set of parameters Θ . \tilde{g}_Θ is assumed to approximate g , to be fast to compute, and to be able to evaluate the reliability of its own predictions in terms of a variance. It is used to explore \mathbf{A} quickly in search of a solution of $\mathbf{z}^* = \operatorname{argmin}_{\mathbf{z} \in \mathbf{A}} g(\mathbf{z})$. Given an initial training set $\{(\mathbf{z}_i, r_i)\}_i$ of input vectors \mathbf{z}_i and outputs $r_i = g(\mathbf{z}_i)$, it iterates the following steps:

1. Find Θ that yields the best possible prediction by \tilde{g}_Θ .
2. Generate new samples not present in the training set.
3. Evaluate an *acquisition function* on these samples.
4. Add the best ones to the training set and go to step 1.

An effective approach to generating the new samples is to apply a genetic algorithm (Gosselin, Tye-Gingras, and Mathieu-Potvin 2009) to the surrogate model \tilde{g}_Θ , which is much faster than applying it to the original function g . For each new sample \mathbf{z} , one must compute the acquisition function. It is often taken to be the *Expected Improvement* (EI), which, in essence, tries to find the point that minimizes the distance to the objective evaluated at the maximum and un-

der Gaussian assumptions can be written as

$$EI(\mathbf{z}) = (\tilde{r} - g(\mathbf{z}^+) - \epsilon) \Phi(Z) + \tilde{\sigma} \phi(Z), \quad (1)$$

$$Z = \frac{\tilde{r} - g(\mathbf{z}^+) - \epsilon}{\tilde{\sigma}},$$

where \tilde{r} is the value predicted by \tilde{g}_Θ , $\tilde{\sigma}$ is the corresponding standard deviation, \mathbf{z}^+ is the best exemplar found so far, $\Phi(\cdot)$ is cumulative distribution function (CDF) and $\phi(\cdot)$ is probability density function (pdf) of standard Gaussian distribution, $\epsilon \in \mathbb{R}$ is a hyperparameter.

3 Method

In this section, we introduce our *DEBOSH* approach to shape optimization. As depicted by Fig. 2, the algorithm iterates the following steps:

1. Given a set of shapes, run physical simulations on each one.
2. Use the training shapes and the simulation results to train one GCNN, or more, to emulate the physical simulations.
3. Generate new shapes and use GCNN(s) to evaluate their acquisition function, as described in 2.2.
4. Add the best new shapes to the set of shapes and iterate.

These four steps are performed either a preset number of times or until reaching given optimization objectives. The main obstacle to implementing this scheme is that GCNNs do not naturally return the uncertainties that evaluation of the acquisition function requires. We overcome it using either MC-Dropout (Gal and Ghahramani 2016b) or Deep Ensembles (Lakshminarayanan, Pritzel, and Blundell 2017), as described below.

3.1 Training Set

Given a set of N 3D shapes $\{\mathbf{x}_i\}_{1 \leq i \leq N}$ represented by triangulated meshes, we run a physics-based simulator numerical solver to create a corresponding set $\{\mathbf{y}_i\}_{1 \leq i \leq N}$ of physical values, such as pressure or mechanical stress at each vertex. Given a field \mathbf{y} , we derive a performance value $r = \mathbf{R}(\mathbf{y})$, such as overall drag for a car or maximum stress for a mechanical part, using a function \mathbf{R} that is task-specific. Assuming that each mesh \mathbf{x} is parameterized by a low-dimensional latent vector \mathbf{z} and that there is a differentiable mapping $\mathbf{P} : \mathbf{z} \rightarrow \mathbf{x}$, this gives us the initial training set $\{(\mathbf{z}_i, r_i)\}_i$ that we need to initialize Bayesian Optimization, as described in Section 2.2.

The \mathbf{x}_i are represented by triangulated meshes with vertices and edges (V_i, E_i) , along with node and edge attributes $\{\mathbf{u}_i^j \in \mathbb{R}^M\}_{j=1}^{|V_i|}$ and $\{\mathbf{v}_i^j \in \mathbb{R}^L\}_{j=1}^{|E_i|}$, where M and L are the dimensions of these attributes. In practice, we take \mathbf{u}_i^j to be the concatenation of vertex's xyz -coordinates with the result of the sinusoidal transformation $\{(\sin ax, \sin ay, \sin az)\}_{a=1}^A$ of these coordinates to encode high frequencies. Edge features \mathbf{v}_i^j are the difference of xyz -coordinates of nodes belonging to a given edge.

3.2 Emulator Architecture

Given the training set of Section 3.1, we train a GCNN (Monti et al. 2017) to predict the field of physical values \mathbf{y} given a mesh \mathbf{x} , as depicted by Fig. 3. The forward pass through a single layer can be written as

$$\tilde{\mathbf{u}}_i^j = \frac{1}{|\mathcal{N}(j)|} \sum_{n \in \mathcal{N}(j)} \frac{1}{K} \sum_{k=1}^K \mathbf{w}_k(\mathbf{v}_i^{j,n}) \otimes \Theta_k \mathbf{u}_i^j \quad (2)$$

where $\mathcal{N}(j)$ is the neighborhood of the j -th node and

$$\mathbf{w}_k(\mathbf{e}) = \exp\left(-\frac{1}{2}(\mathbf{e} - \mu_k)^T \Sigma_k^{-1}(\mathbf{e} - \mu_k)\right) \quad (3)$$

denotes a weighting function based on trainable mean vector μ_k and diagonal covariance matrix Σ_k^{-1} . Such a layer involves three types of trainable weights: $\Theta_k \in \mathbb{R}^{\tilde{L} \times L}$ maps input \mathbf{u}_i^j to the new dimensionality, and μ_k and Σ_k define the Gaussian kernel used to convolve a node with its neighbors. Our final model consists of 25 GNN layers with ELU nonlinearities (Clevert, Unterthiner, and Hochreiter 2015) and skip connections (He et al. 2016).

3.3 Bayesian Optimization

Recall from Section 2.2 that Bayesian Optimization (BO) is an exploration-and-exploitation approach to minimizing a function g given a trainable estimator \tilde{g}_Θ that can evaluate its own uncertainty. In our case, g is the function that takes as input a latent vector \mathbf{z} , produces a triangulated mesh $\mathbf{x} = \mathbf{P}(\mathbf{z})$, computes the associated field of physical values \mathbf{y} using a simulator, and finally outputs a performance value $r = \mathbf{R}(\mathbf{y})$.

We now need to define \tilde{g}_Θ . Given a latent vector \mathbf{z} and the GCNN of Section 3.2 with weights Θ , we can approximate the performance by feeding the triangulated mesh $\mathbf{P}(\mathbf{z})$ to the network to produce an estimated field of values $\tilde{\mathbf{y}}$ and an estimated performance value $\tilde{r} = \mathbf{R}(\tilde{\mathbf{y}})$. We take this to be the estimate that \tilde{g}_Θ but we also need an uncertainty estimate in the form of a variance, which means assessing the reliability of our network. Among all the methods that can be used to assess to this end, MC-Dropout (Gal and Ghahramani 2016b) and Deep Ensembles (Lakshminarayanan, Pritzel, and Blundell 2017) have emerged as two of the most popular ones. MC-Dropout involves randomly zeroing out network weights and assessing the effect, whereas Ensembles involve training multiple networks starting from different initial conditions. In practice, the latter tends to perform better but also to be more computationally demanding due to the requirement of restarting the training procedure from scratch many times.

In practice, we implemented both approaches. For ensembles approaches, for each training set, we train the N different networks with weights $\Theta_1, \dots, \Theta_n$ and use the mean and variance of the estimates

$$\mu(\mathbf{z}) = \frac{1}{N} \sum_{i=1}^N \tilde{\mathbf{g}}_{\Theta_i}(\mathbf{x}), \quad (4)$$

$$\sigma^2(\mathbf{z}) = \frac{1}{N-1} \sum_{i=1}^N (\tilde{\mathbf{g}}_{\Theta_i}(\mathbf{x}) - \mu(\mathbf{x}))^2.$$

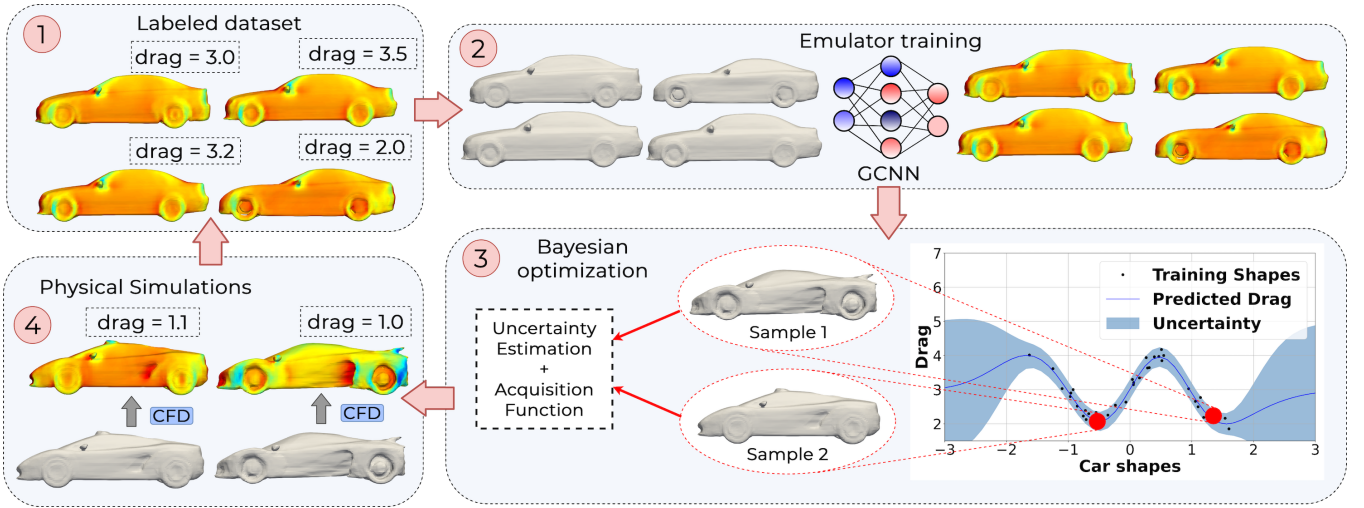


Figure 2: **DEBOSH pipeline**: (1) Run physical simulations. (2) Train the GCNN. (3) Perform Bayesian Optimization. (4) Select promising samples, add them to the training set, and go back to step 1.

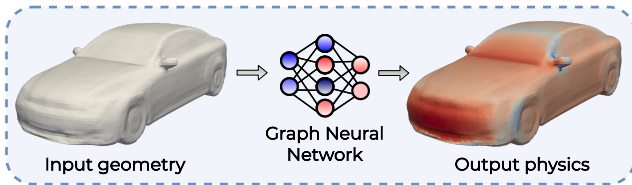


Figure 3: **Emulation model for pressure prediction**. Given an input geometry mesh our GCNN outputs a field of pressure values on the sample’s surface without having to run a computationally expensive simulation.

For MC-Dropout, we proceed similarly but, instead of using different weights Θ_i , we run the inference several times to get multiple estimates, along with their mean and variance.

4 Experiments

In this section, we compare *DEBOSH* against state-of-the-art alternatives in several scenarios.

4.1 Baselines and Variants

We will compare four different approaches to performing shape optimization, which we describe briefly below.

- *Kriging*: Using a GP to estimate a response surface and corresponding uncertainty from a number of shape exemplars and corresponding simulations results is known as Kriging (Laurenceau et al. 2010). This response surface can then be used to optimize shapes using Bayesian Optimization. As discussed in Section 2.1, it is a widely used practice and is a standard approach to BO.
- *GCNN*: An alternative to using GPs to estimate the response surface is to use a standard GCNN (Baqué et al. 2018; Remelli et al. 2020), as discussed in Section 2.1. Since a GCNN does not return uncertainties, the optimization is performed using deterministic gradient-descent.

	<i>Kriging</i>	<i>GCNN</i>	<i>Ours-MCD</i>	<i>Ours-Ens</i>
Foils : Lift-to-Drag	1.62	1.81	1.94	2.08
Cars : Drag	3.4	2.8	2.6	2.3
Knuckles : Stress	105.	100.	95.	91.

Table 1: **Optimized fitness values for airfoils, cars, and knuckles**. Highest lift-to-drag and lowest drag and stress values for the three types of shapes we tested all four methods on. *Ours-Ens* systematically delivers the best values with *Ours-MCD* being second best.

- *Ours-MCD*: Our method when using MC-Dropout to estimate uncertainties.
- *Ours-Ens*: Our method when using deep ensembles to estimate uncertainties.

We report the results obtained by all four methods on three different types of optimization problems in Table. 1. *Ours-Ens* clearly outperforms the other approaches with *Ours-MCD* being second best. In other words, using a GCNN to estimate both the fitness of a shape and the corresponding uncertainty is beneficial and using ensembles is even more so than using drop-out. We discuss how we obtained these results in more details below.

4.2 2D Airfoil Optimization

2D airfoil profile optimization has become a *de facto* standard for benchmarking shape optimization in the CFD community. In industrial practice, profiles have long been parameterized using a three-dimensional NACA parameter vector (Jacobs, Ward, and Pinkerton 1948) and optimized using conventional Kriging-based methods (Jeong, Murayama, and Yamamoto 2005; Chiplunkar, Bosco, and Morlier 2017). We generated an initial dataset of 200 shapes for airfoil optimization by randomly selecting NACA parameters \mathbf{z}_i and then producing corresponding 2D contours \mathbf{x}_i for each one.

We use the popular XFOIL simulator (Drela 1989) to compute the pressure distribution \mathbf{y}_i over the surface of each \mathbf{x}_i .

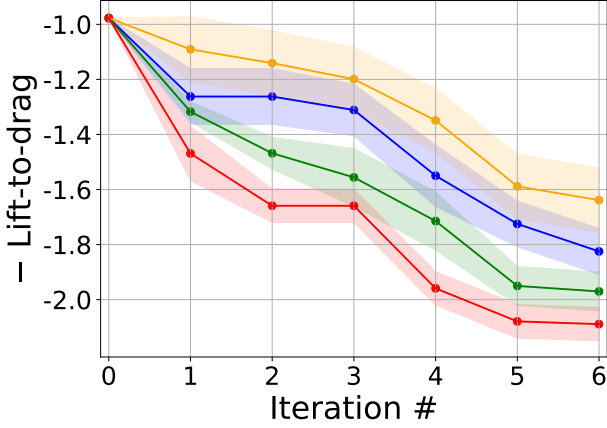


Figure 4: **Lift-to-drag maximization for airfoils.** We ran each training procedure 5 times with different random seeds. Each line represents the average negative lift-to-drag-ratio of the best performing profile as a function of the number of training iterations. The shaded areas depict the corresponding variances. They are color coded according to the method used to perform the minimization, *Ours-Ens*, *Ours-MCD*, *Kriging*, and *GCNN*. The *Ours-Ens* curve is below the others.

Even though GCNNs models are primarily designed to handle 3D shapes, they can also handle 2D ones by considering the 2D equivalent of a surface mesh, which is a discretized 2D contour. As in (Baqué et al. 2018), train one to predict pressure values \tilde{y}_i at each vertex along with the overall lift-to-drag ratio, which we take to be $R(\mathbf{y}_i)$, which could also be obtained by integrating the pressure values over the surface of the shape.

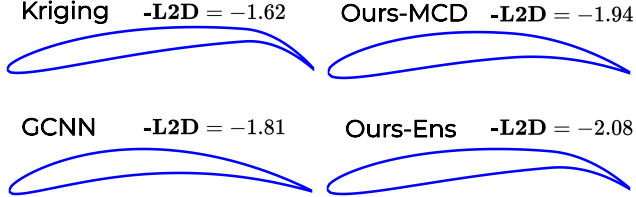


Figure 5: **Optimized 2D wing profiles.** Best performing profile found by each one of the four methods we tested.

As discussed in Section 3.3, for *Ours-Ens* we train five GCNNs at each iteration while we train only one *Ours-MCD*. In both cases, after each training iteration, we use the genetic algorithm NSGAI (Deb et al. 2002) coupled to the GCNN(s) to sample 30 new airfoil shapes and to evaluate the corresponding acquisition function. For *Kriging*, we proceed similarly but use GPs instead of a GCNN to run the generic algorithm and evaluate the acquisition function. For *GCNN*, we use the network to predict lift-to-drag values $R(\tilde{\mathbf{y}}_i)$ and pick sampled shapes for simulations according to this metric instead of the acquisition function, which would require an uncertainty estimate.

Fig. 4 depicts the lift-to-drag-ratios for all four approaches

as function of the number of training iterations. Fig. 5 depicts the best foils found by each one of the four approaches. We report the corresponding lift-to-drag ratios in Table 1.

4.3 Minimizing Car Drag

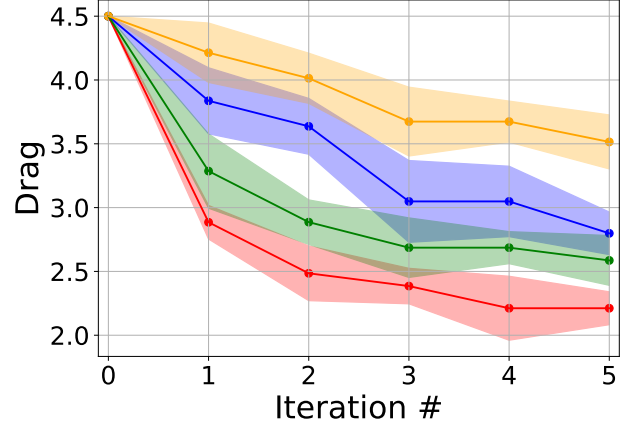


Figure 6: **Drag minimization for cars.** As in Fig. 4, the individual curves are color coded. They represent drag values and their variances as a function of the number of training iterations for *Ours-Ens* and *Ours-MCD*, *Kriging*, and *GCNN*. The *Ours-Ens* curve is again below the others.

Even though airfoil optimization using the NACA parameterization is a standard benchmark, it relies on a 3-Dimensional latent vector and is therefore very low-dimensional. We now turn to a higher-dimensional problem in which the latent vector is of dimension 256: car-shape optimization to minimize drag.

As in (Remelli et al. 2020), we use a cleaned-up and processed subset of the ShapeNet dataset (Chang et al. 2015) that features $N = 1400$ car meshes that are suitable for CFD simulation. For each such mesh \mathbf{x}_i , we run OpenFOAM (Jasak et al. 2007) to estimate the pressure field \mathbf{y}_i created by air travelling at 15 meters per second towards the car. We also train the MeshSDF (Remelli et al. 2020) mapping \mathbf{P} on this training dataset so that for each \mathbf{x}_i there is 256-dimensional latent vector \mathbf{z}_i such that $\mathbf{x}_i = \mathbf{P}(\mathbf{z}_i)$. Though many mesh and graph embedding methods were proposed recently in literature (Park et al. 2019; Mescheder et al. 2019; Ivanov, Durasov, and Burnaev 2018; Baqué et al. 2018), MeshSDF proved to be one of the most efficient and expressive in CFD context.

Given such a training set, we can train a GCNN such as the one of Section 3.2 to predict a pressure field $\tilde{\mathbf{y}}$ that approximates the true one for a car shape $\mathbf{x} = \mathbf{P}(\mathbf{z})$. Its drag can be approximated by the surface integral

$$D(\tilde{\mathbf{y}}) = \iint_S \tilde{y} \mathbf{n}_x dS, \quad (5)$$

where \mathbf{n}_x denotes the projection of the surface normals along the airflow direction and \tilde{y} is the scalar value of the pressure field at a given surface point.

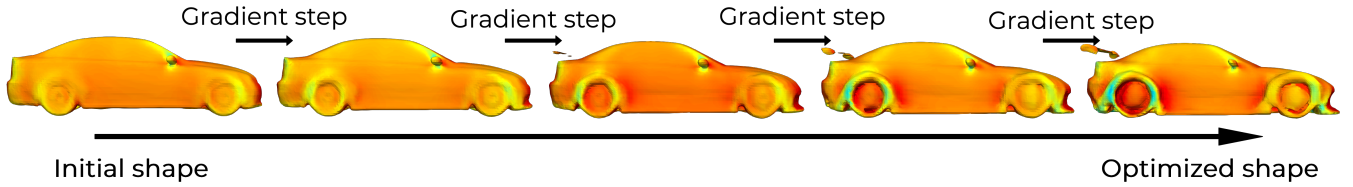


Figure 7: **Gradient descent-based drag minimization.** Starting from the initial shape on the left, $R(\tilde{\mathbf{z}})$ from Eq. 6 is minimized with respect to \mathbf{z} using gradient descent steps. The middle shapes depict the optimization process and the relative improvements in terms of defined $R(\tilde{\mathbf{z}})$. The final result is shown on the right. The mapping \mathbf{P} of (Remelli et al. 2020) enforces implicit semantic priors while being able to effect topology changes that result in plausible cars shapes.

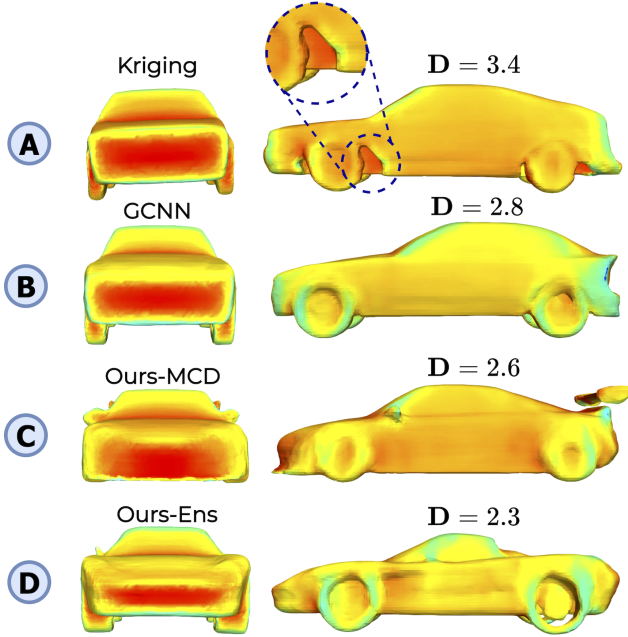


Figure 8: **Optimized 3D car shapes.** Best car shapes found by each one of the four methods we tested. (A) *Kriging* (B) *GCNN* (C) *Ours-MCD* (D) *Ours-Ens*. Note the artifact produced by *Kriging* that the other methods do not produce. Note also, that the topology of the *Ours-MCD* and *Ours-Ens* cars are different, which is made possible by the fact that the latent representation we use allows topology changes.

We could take D to be the function we minimize but all the shapes would reduce to a point. Instead, we write

$$R(\tilde{\mathbf{z}}) = D(\tilde{\mathbf{y}}) + R_{aux}(\mathbf{z}), \quad (6)$$

where R_{aux} is a penalty term that becomes large if the car shape strays away too much from those in the training set. In practice, we take it to be the average Euclidean distance to the five closest neighbors of \mathbf{z} in the training set. During minimization, keeping R_{aux} forces \mathbf{z} to remain close from the parts of the shape space for which the parameterizer \mathbf{P} has been trained and to keep on generating plausible cars. Adding this penalty term constrains the exploration of the latent space but guarantees more robust and realistic optimization outcomes.

When performing BO to minimize R , we could use a genetic algorithm to create new samples as we did for the air

foils. However, we now have to explore a 256-dimensional shape space, and each evaluation of the surrogate model, while much faster than an actual simulation, requires computing \mathbf{P} . This involves running the Marching Cube algorithms to compute the mesh vertices (Lorensen and Cline 1987), which takes time and makes vanilla genetic algorithms very slow.

Instead, we take advantage of the fact that, even though the Marching Cube algorithms is non-differentiable, the mapping \mathbf{P} is differentiable (Guillard et al. 2021) as follows. At each training iteration, we start from the existing elements of the training set and perform gradient descent using them as a starting point. Fig. 7 depicts this process. This gives a new set of shapes and we select the best ones according to the acquisition function, as in standard BO.

Fig. 6 depicts the resulting drag coefficients for all four approaches as function of the number of training iterations. Again, *Ours-Ens* outperforms the other approaches, followed by *Ours-MCD*. We report the final numbers in Table 1 and the corresponding car shapes are shown in Fig. 8.

4.4 Mechanical Stress Minimization

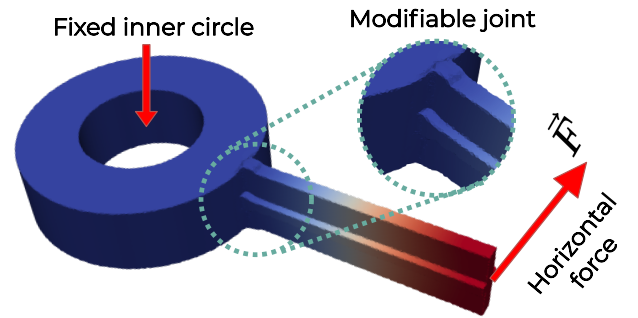


Figure 9: **Stress minimization problem.** The plot represents a setup for stress prediction and minimization for special detail called *knuckle*. Horizontal force \vec{F} applied to the tip of the handle induces tension distributed throughout the entire volume of the detail. Proper design of the joint is required to produce durable and long-lasting construction.

To show that we can handle a very different kind of problem, we now consider a structural engineering problem. Our goal is to minimize the mechanical stresses in the *knuckle*

depicted by Fig. 9. It is made of a metal ring with a long handle attached to it. Fixing the inner circle of the ring and applying a horizontal force to the handle tip creates mechanical stress. Minimizing it is desirable because it significantly extends the lifespan of the part and can be achieved by shaping properly the most fragile part, which is the joint between the handle and the ring.

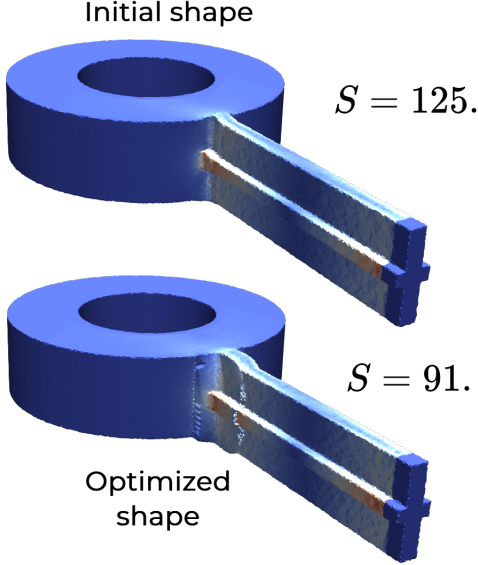


Figure 10: **Optimized 3D knuckle.** Starting from 3D shapes such as the one at the top, *Ours-Ens* searches for optimized RBF parameters to strengthen the joint between the handle and the ring, the most fragile part of the assembly. The final result is shown at the bottom. As expected, the method makes the joint heavier and therefore better able to handle the external force \vec{F} .

To test this, we have generated $N = 200$ knuckle shapes with different joint configurations. Variation in joint shapes is parametrized using the Radial Basis Function (RBF) parametrizer (Forti and Rozza 2014) \mathbf{P} that relies on control points and RBF interpolation. For each shape \mathbf{x}_i , we use a finite element solver (Cimrman 2021) that computes the von Mises stresses \mathbf{y}_i across the joint and we write

$$R(\mathbf{y}_i) = \max_i \mathbf{y}_i. \quad (7)$$

Since the latent vector is of dimension 9, we use the same approach to BO as for the airfoil. At every training iteration, we sample 30 new shapes and use the acquisition function to retain 10 shapes and add them to original training dataset. Fig. 11 depicts the resulting stresses for all four approaches as function of the number of training iterations. Again, *Ours-Ens* outperforms the other approaches. We report the final numbers in Table 1 and show the best final shape in Fig. 10.

5 Conclusion

In this work, we have shown that neural networks could be used as surrogate models for Bayesian Optimization. We have demonstrated on several realistic scenarios that using

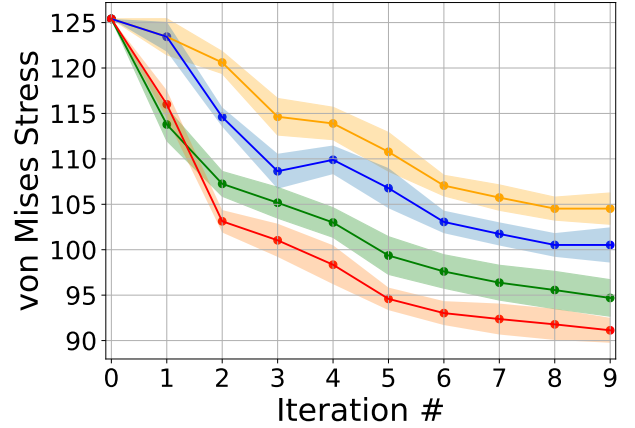


Figure 11: **Stress minimization for knuckles.** As in Fig. 4, the individual curves are color coded. They represent stress values and their variances as a function of the number of training iterations for *Ours-Ens* and *Ours-MCD*, *Kriging*, and *GCNN*. The *Ours-Ens* curve is again below the others.

either MC-dropout or deep ensembles is an effective way to estimate the uncertainty of the network’s prediction, which is a key ingredient of BO. MC-Dropout tends to be faster but Ensembles deliver better results. In future work, we will focus on developing approaches to estimating uncertainty that combine the accuracy of Ensembles with the speed of MC-dropout.

References

- Alexandersen, J.; Sigmund, O.; and Aage, N. 2016. Large Scale Three-Dimensional Topology Optimization of Heat Sinks Cooled by Natural Convection. *International Journal of Heat and Mass Transfer*, 100(Supplement C): 876–891.
- Allaire, G. 2015. A Review of Adjoint Methods for Sensitivity Analysis, Uncertainty Quantification and Optimization in Numerical Codes. *Ingénieurs de l’Automobile*, 836: 33–36.
- Baqué, P.; Remelli, E.; Fleuret, F.; and Fua, P. 2018. Geodesic Convolutional Shape Optimization. In *International Conference on Machine Learning*.
- Behrou, R.; Ranjan, R.; and Guest, J. K. 2019. Adaptive Topology Optimization for Incompressible Laminar Flow Problems with Mass Flow Constraints. *Computer Methods in Applied Mechanics and Engineering*, 346: 612–641.
- Bellman, R. 1961. *Curse of Dimensionality*. Princeton university press.
- Boscaini, D.; Masci, J.; Rodolà, E.; and Bronstein, M. 2016. Learning Shape Correspondence with Anisotropic Convolutional Neural Networks. In *Advances in Neural Information Processing Systems*, 3189–3197.
- Chang, A.; Funkhouser, T.; G., L.; Hanrahan, P.; Huang, Q.; Li, Z.; Savarese, S.; Savva, M.; Song, S.; Su, H.; Xiao, J.; Yi, L.; and Yu, F. 2015. Shapenet: An Information-Rich 3D Model Repository. In *arXiv Preprint*.

- Chen, L.-C.; Papandreou, G.; Kokkinos, I.; Murphy, K.; and Yuille, A. L. 2017. Deeplab: Semantic image segmentation with deep convolutional nets, atrous convolution, and fully connected crfs. *IEEE transactions on pattern analysis and machine intelligence*, 40(4): 834–848.
- Chiplunkar, A.; Bosco, E.; and Morlier, J. 2017. Gaussian Process for Aerodynamic Pressures Prediction in Fast Fluid Structure Interaction Simulations. In *World Congress of Structural and Multidisciplinary Optimisation*, 221–233.
- Cimrman, R. 2021. Fast Evaluation of Finite Element Weak Forms Using Python Tensor Contraction Packages. *Advances in Engineering Software*, 159.
- Clevert, D.-A.; Unterthiner, T.; and Hochreiter, S. 2015. Fast and accurate deep network learning by exponential linear units (elus). *arXiv preprint arXiv:1511.07289*.
- Deb, K.; Pratap, A.; Agarwal, S.; and Meyarivan, T. 2002. A fast and elitist multiobjective genetic algorithm: NSGA-II. *IEEE transactions on evolutionary computation*, 6(2): 182–197.
- Drela, M. 1989. XFOIL: An Analysis and Design System for Low Reynolds Number Airfoils. In *Conference on Low Reynolds Number Aerodynamics*, 1–12.
- Durasov, N.; Bagautdinov, T.; Baque, P.; and Fua, P. 2021. Masksembles for Uncertainty Estimation. In *Conference on Computer Vision and Pattern Recognition*.
- Durasov, N.; Romanov, M.; Bubnova, V.; Bogomolov, P.; and Konushin, A. 2019. Double Refinement Network for Efficient Monocular Depth Estimation. In *2019 IEEE/RSJ International Conference on Intelligent Robots and Systems (IROS)*, 5889–5894.
- Forti, D.; and Rozza, G. 2014. Efficient geometrical parametrisation techniques of interfaces for reduced-order modelling: application to fluid–structure interaction coupling problems. *International Journal of Computational Fluid Dynamics*, 28(3-4): 158–169.
- Gal, Y.; and Ghahramani, Z. 2016a. Dropout as a bayesian approximation: Representing model uncertainty in deep learning. In *international conference on machine learning*, 1050–1059. PMLR.
- Gal, Y.; and Ghahramani, Z. 2016b. Dropout as a Bayesian Approximation: Representing Model Uncertainty in Deep Learning. In *International Conference on Machine Learning*, 1050–1059.
- Gao, Y.; Wu, Y.; and Xia, J. 2017. Automatic Differentiation Based Discrete Adjoint Method for Aerodynamic Design Optimization on Unstructured Meshes. *Chinese Journal of Aeronautics*, 30(2): 611–627.
- Gosselin, L.; Tye-Gingras, M.; and Mathieu-Potvin, F. 2009. Review of Utilization of Genetic Algorithms in Heat Transfer Problems. *International Journal of Heat and Mass Transfer*, 52(9): 2169–2188.
- Guillard, B.; Remelli, E.; Lukoianov, A.; Richter, S.; Bagautdinov, T.; Baque, P.; and Fua, P. 2021. DeepMesh: Differentiable Iso-Surface Extraction. *arXiv Preprint*.
- Guo, X.; Li, W.; and Iorio, F. 2016. Convolutional Neural Networks for Steady Flow Approximation. In *Proceedings of the 22nd ACM SIGKDD International Conference on Knowledge Discovery and Data Mining*, KDD '16, 481–490. New York, NY, USA: Association for Computing Machinery. ISBN 9781450342322.
- He, K.; Zhang, X.; Ren, S.; and Sun, J. 2016. Deep residual learning for image recognition. In *Proceedings of the IEEE conference on computer vision and pattern recognition*, 770–778.
- Herbrich, R.; Lawrence, N.; and Seeger, M. 2003. Fast Sparse Gaussian Process Methods: The Informative Vector Machine. In *Advances in Neural Information Processing Systems*, 625–632.
- Ivanov, S.; Durasov, N.; and Burnaev, E. 2018. Learning node embeddings for influence set completion. In *2018 IEEE International Conference on Data Mining Workshops (ICDMW)*, 1034–1037. IEEE.
- Jacobs, E.; Ward, K.; and Pinkerton, R. 1948. The Characteristics of 78 Related Airfoil Sections from Tests in the Variable Density Wind Tunnel. Technical report.
- Jasak, H.; Jemcov, A.; Tukovic, Z.; et al. 2007. OpenFOAM: A C++ library for complex physics simulations. In *International workshop on coupled methods in numerical dynamics*, volume 1000, 1–20.
- Jeong, S.; Murayama, M.; and Yamamoto, K. 2005. Efficient Optimization Design Method Using Kriging Model. *Journal of Aircraft*, 42(2): 413–420.
- Kim, B.; Azevedo, V. C.; Thuerey, N.; Kim, T.; Gross, M.; and Solenthaler, B. 2019. Deep fluids: A generative network for parameterized fluid simulations. In *Computer Graphics Forum*, 59–70.
- Lakshminarayanan, B.; Pritzel, A.; and Blundell, C. 2017. Simple and Scalable Predictive Uncertainty Estimation Using Deep Ensembles. In *Advances in Neural Information Processing Systems*.
- Laurenceau, J.; Meaux, M.; Montagnac, M.; and Sagaut, P. 2010. Comparison of Gradient-Based and Gradient-Enhanced Response-Surface-Based Optimizers. *American Institute of Aeronautics and Astronautics Journal*, 48(5): 981–994.
- Liu, W.; Durasov, N.; and Fua, P. 2021. Leveraging Self-Supervision for Cross-Domain Crowd Counting. *arXiv preprint arXiv:2103.16291*.
- Lorensen, W.; and Cline, H. 1987. Marching Cubes: A High Resolution 3D Surface Construction Algorithm. In *ACM SIGGRAPH*, 163–169.
- Mescheder, L.; Oechsle, M.; Niemeyer, M.; Nowozin, S.; and Geiger, A. 2019. Occupancy networks: Learning 3d reconstruction in function space. In *Proceedings of the IEEE/CVF Conference on Computer Vision and Pattern Recognition*, 4460–4470.
- Mockus, J. 2012. *Bayesian approach to global optimization: theory and applications*, volume 37. Springer Science & Business Media.

Monti, F.; Boscaini, D.; Masci, J.; Rodolà, E.; Svoboda, J.; and Bronstein, M. M. 2017. Geometric Deep Learning on Graphs and Manifolds Using Mixture Model CNNs. In *Conference on Computer Vision and Pattern Recognition*, 5425–5434.

Mountrakis, L.; Lorenz, E.; Malaspinas, O.; Alowayyed, S.; Chopard, B.; and Hoekstra, A. 2015. Parallel Performance of an IB-LBM Suspension Simulation Framework. *Journal of Computational Science*.

Park, J. J.; Florence, P.; Straub, J.; Newcombe, R.; and Lovegrove, S. 2019. DeepSDF: Learning continuous signed distance functions for shape representation. In *Proceedings of the IEEE/CVF Conference on Computer Vision and Pattern Recognition*, 165–174.

Rasmussen, C. E.; and Williams, C. K. 2006. *Gaussian Process for Machine Learning*. MIT Press.

Redmon, J.; Divvala, S.; Girshick, R.; and Farhadi, A. 2016. You only look once: Unified, real-time object detection. In *Proceedings of the IEEE conference on computer vision and pattern recognition*, 779–788.

Remelli, E.; Lukoianov, A.; Richter, S.; Guillard, B.; Bagautdinov, T.; Baque, P.; and Fua, P. 2020. MeshSdf: Differentiable Iso-Surface Extraction. In *Advances in Neural Information Processing Systems*.

Saviers, K. R.; Ranjan, R.; and Mahmoudi, R. 2019. Design and Validation of Topology Optimized Heat Exchangers. In *AIAA Scitech 2019 forum*, 1465.

Toal, D.; and Keane, A. 2011. Efficient Multipoint Aerodynamic Design Optimization via Cokriging. *Journal of Aircraft*, 48(5): 1685–1695.

Tompson, J.; Schlachter, K.; Sprechmann, P.; and Perlin, K. 2017. Accelerating eulerian fluid simulation with convolutional networks. In *International Conference on Machine Learning*, 3424–3433. PMLR.

Umetani, N.; and Bickel, B. 2018. Learning Three-Dimensional Flow for Interactive Aerodynamic Design. *ACM Transactions on Graphics*, 37(4): 89.

Vaswani, A.; Shazeer, N.; Parmar, N.; Uszkoreit, J.; Jones, L.; Gomez, A. N.; Kaiser, Ł.; and Polosukhin, I. 2017. Attention is all you need. In *Advances in neural information processing systems*, 5998–6008.

Weller, H. G.; Tabor, G.; Jasak, H.; and Fureby, C. 1998. A Tensorial Approach to Computational Continuum Mechanics Using Object-Oriented Techniques. *Computational Physics*, 12(6): 620–631.

Wen, Y.; Tran, D.; and Ba, J. 2020. Batchensemble: an alternative approach to efficient ensemble and lifelong learning. *arXiv preprint arXiv:2002.06715*.

Xu, G.; Liang, X.; Yao, S.; Chen, D.; and Li, Z. 2017. Multi-Objective Aerodynamic Optimization of the Streamlined Shape of High-Speed Trains Based on the Kriging Model. *PloS one*, 12(1): 1–14.